Received: 19 August 2020 | Revised: 16 December 2020 | Accepted: 19 January 2021

DOI: 10.1002/aic.17225

TRANSPORT PHENOMENA AND FLUID MECHANICS

AIChE JOURNAL

Effect of hydrodynamic heterogeneity on micromixing intensification in a Taylor–Couette flow reactor with variable configurations of inner cylinder

Lu Liu[1] | Xiaogang Yang[1] | Jie Yang[2] | Guang Li[1] | Yanqing Guo[1]

[1]Department of Mechanical, Materials and Manufacturing Engineering, University of Nottingham Ningbo China, Ningbo, China

[2]Department of Physics and Mathematics, University of Hull, Hull, UK

Correspondence
Xiaogang Yang, Department of Mechanical, Materials and Manufacturing Engineering, University of Nottingham Ningbo China, Ningbo 315100, China.
Email: xiaogang.yang@nottingham.edu.cn

Funding information
National Natural Science Foundation of China, Grant/Award Numbers: 21606259, 21576141, 21761132026

Abstract

Effect of hydrodynamic heterogeneity on micromixing intensification in a Taylor–Couette flow (TC) reactor with variable configurations of inner cylinder has been investigated by adoption of a parallel competing iodide-iodate reaction system. Two types of inner cylinder, circular inner cylinder and lobed inner cylinder (CTC and LTC), were used to generate hydrodynamic heterogeneity, focusing on the effects of the Reynolds number, the acid concentration, and the feeding time on the micromixing performance. Segregation index (*Xs*) was employed to evaluate the micromixing efficiency. It is revealed that *Xs* decreases with the increase of Reynolds number and feeding time but increases with the increase of acid concentration for both the CTC and LTC. However, the LTC does present a better micromixing performance at various operating conditions than that of the CTC as affirmed by both the experimental and computational fluid dynamics simulation results.

KEYWORDS
geometry modification, micromixing efficiency, micromixing time, segregation index

1 | INTRODUCTION

During the synthesis of various micro/nano particles, the hydrodynamics of the mixing in reactors has been recognized as playing a determinant role in determining the synthesized particle properties. In particular, micromixing, which takes place at the molecular scale, has been considered as the rate determining step during chemical reaction, especially for the fast chemical reactions involved as pointed out by Baldyga.[1] Fast chemical reactions often have the similar or even lower time scale than that of the micromixing. Under such conditions, reactions have been already completely before reactants reach a homogenous mixing. In some cases, even mixing is deemed to be effective at the macro scale, it may not have achieved homogeneity at the micro scale yet. As a perfect micromixing condition can effectively increase the yield of the desired particle and reduce by-products at the same time, the improvement of micromixing will be beneficial to the intensification of particle synthesis process, given that particle precipitation is often an instantaneous process.

Various kinds of reactor have been developed and investigated in previous studies, aiming to improve the mixing performance. For example, the use of a spinning disk reactor,[2] impinging jet reactor,[3] microchannel reactor,[4] T-shaped reactor,[5] and high shear mixer[6] have all been studied before. The Taylor–Couette flow (TC) reactor with the features of controllable mean residence time and narrow shear rate distribution has also received a lot of attention. This type of reactor has a simple configuration, where the inner cylinder rotates relative to the outer one. Jung et al[7] prepared calcium carbonate particles by a gas–liquid reaction system using a TC reactor, and obtained three particle morphologies (cube-like, transition and spindle). They attempted to introduce an enhancement factor correlated with the

mass transfer rate to characterize this type of behavior, and suggested that the particle shape change depends on this enhancement factor. Tang et al[8] have investigated the morphology change of copper sulfide nanoparticles by using the TC reactor and found that an intensified mass transfer rate can be achieved using such reactor. By tracing the other applications, Kim and his co-researchers have employed the TC reactor to synthesize many types of fine particles, such as cathode precursors for lithium ion batteries,[9,10,11] barium sulfate,[12] L-histidine,[13] and Guanosine 5-monophosphate.[14] Their work mainly focused on the applications of the TC reactor during particle synthesis process. However, these studies lacked the fundamental investigation of the mechanisms involved behind the mixing, mass transfer and heat transfer processes.

During particle synthesis process, many previous studies have indicated that even a minor change of reactor configuration will lead to a significant effect on the micromixing performance. Jacobsen and Hinrichsen[2] investigated the micromixing characteristics in a spinning disk reactor with different feeding locations and surface structures, and used the synthesized barium sulfate particles for validation. Zhu et al[15] synthesized cathode precursor $Ni_{0.6}Co_{0.2}Mn_{0.2}(OH)_2$ for lithium ion batteries in a stirred tank with four different types of impeller. They finally obtained particles with different shapes and tap densities and consequently, different electrochemical performances. They attributed these differences to the different flow fields generated by four impellers. All these previous studies have revealed that geometrical optimization is an effective and economical approach to improve the performance of these existing reactors. As mentioned earlier, TC reactor has many features that are beneficial to the particle synthesis. However, the shear regions in the TC reactor are not locally uniformly distributed. In order to better utilize the advantage of overall shear control, the modification of the classical TC reactor has been suggested. Soos et al[16] proposed a lobed profile for the inner cylinder in order to reduce the low velocity gradient region. They found that this configuration can successfully enhance the local shear rate in the vicinity of the inner cylinder. Li et al[17] have compared the mixing performance in the TC reactor with various cross-sectional profiles of inner cylinder including a lobed one using CFD simulation in terms of flow patterns, shear strain rate distribution and micromixing time. They ascertained that the mixing performance improves when using the lobed profile. With respect to its application to particle synthesis process, the aggregation of sulfate polystyrene latex particles with a mean diameter of 600 nm was investigated in Ehrl et al's[18] work by comparing the stirred tank and TC-type devices. Three cross-sectional geometries were involved with a circular inner cylinder and two lobed inner cylinders. The results indicate that TC device demonstrates its advantages over the stirred tank device in controlling particle size and structure due to the relatively narrow shear distribution, while the difference for the three TC-type devices is marginal. Their work mainly focused on the single process of aggregation, but failing to involve chemical reaction, nucleation and particle growth. Furthermore, Liu et al[19] have reported the synthesis of the barium sulfate particles by using the TC reactor with the classical circular cross-sectional profile inner cylinder and a lobed profile inner cylinder. The experimental results clearly indicate that the properties of the secondary particles (i.e., agglomerates) are different in terms of particle morphology, particle size and its distribution. The aforementioned investigations have implications where the mixing in the TC reactor is significantly affected by the hydrodynamics in the reactor and also by the inner cylinder configuration adopted. Other applications of the lobed TC reactor can be extended to the animal cell cultivation process. Due to the shear sensitivity of animal cells, TC bioreactor often operates at laminar conditions. Santiago et al[20] suggested that Taylor vortex flow regime is suitable to culture animal cells, where oxygen can be sufficiently provided but with a low fluid shear. However, under such conditions, inter-vortex mixing mainly depends on molecular diffusion, which will result in significant heterogeneity.[21] In order to improve the inter-vortex mass transfer, Sorg et al[22] employed a lobed TC reactor to culture cells. They found that this device can easily control the additional power input by avoiding bubble breakup and bursting, and generating a rather homogeneous microenvironment with a narrower shear distribution to facilitate cell metabolism. These results remind us to carefully choose an appropriate flow regimes during cell cultivation.

So far, the micromixing process in the TC reactor has not been clearly understood though a number of experimental work and theoretical studies conducted.[23,24,25] Also, these previous studies have mainly focused on the TC reactors with the circular cross-sectional profile inner cylinder and the modifications on the configuration were mainly subjected to the changes of gap size and aspect ratio.[26,27] The impact of configuration variation on the micromixing performance, especially the inner cylinder alteration, is still rarely studied in the literature. Richter et al[28] compared mixing performance of the classical TC reactor and a novel TC reactor with ribbed rotor assembled in laminar flows with Reynolds numbers smaller than 2.0. In order to test the micromixing performance down to the molecular level, they adopted alkaline saponification of ethylacetate as the reactive system. It is found that ribbed configuration can segregate reactant flows, leading to backmixing. Thus, the authors indicated that configuration modification can be seen as a promising method for process intensification. Similarly, Li et al[17] also suggested that as chemical reactions take place at a molecular level, micromixing may dominate this process. In their work, micromixing time was estimated in the TC reactors by $t_m = \frac{12}{ln2}\sqrt{\frac{\nu}{\varepsilon}}$ with five different inner cylinders including a lobed one, where ε is the turbulent kinetic energy dissipation rate, obtained from CFD modeling results. Compared to the classical TC reactor, the lobed TC reactor shows a rather small micromixing time. Their work mainly focused on CFD modeling technique applied to the TC reactor system, while lacking experimental data to calculate micromixing time.

The aim of the present work is to investigate the micromixing performance in the TC reactor with two different types of inner cylinders and to obtain the guidelines for further enhancing micromixing performance through the configuration modification. A parallel competing system based on the iodide-iodate reaction proposed by Villermaux and co-workers[29,30] has been employed, attempting to

reveal the effects of key operating parameters on the segregation index, which can reasonably serve as an indicator for assessing the micromixing performance. The key parameters include the Reynolds number based on the gap size, the reactant feeding time and the acid concentration. In addition, the micromixing time based on the experimental data by employing the incorporation model are also evaluated and compared.

2 | MICROMIXING CHARACTERIZATION

Various chemical reaction schemes serving as molecular probes have been proposed and commonly accepted by researchers to characterize the micromixing performance for the reaction system involved. Typical systems are single reaction systems ($A + B \rightarrow R$), consecutive reaction systems ($A + B \rightarrow R$, $B + R \rightarrow S$) and parallel competing reaction systems ($A + B \rightarrow R$, $A + C \rightarrow S$). Due to the rigorous conditions imposed for the online analysis of the single reaction, the last two schemes are favoured and usually employed when measuring the final product quality. Bourne and his co-workers proposed several reaction systems based on the consecutive competing scheme, such as the bromination of 1,3,5-trimethoxybenzene,[31] the azo-coupling of 1-naphthol with diazotised sulphanilic acid[32] and the selective iodination of l-tyrosine.[33] However, these proposed systems and the experimental methods still have some disadvantages, especially with their toxic, volatile and unstable nature. With a better understanding of the mixing and chemical reactions, Villermaux et al [34] and Fournier et al[30] proposed the use of a parallel competing scheme based on the iodide-iodate reaction system. Generally, the products produced in such a system are easily analyzed by using the spectrophotometric method. Due to its low toxicity, simple measurement and high sensitivity, such reaction system has been widely adopted to characterize micromixing in mixing devices,[2,35,36,37] especially for fast mixing. Bertrand et al[38] compared the micromixing performance in three high-intensity mixers from the same family but with some geometrical differences, named as T-shaped, Y-shaped tubes and a Hartridge–Roughton mixing device by employing Villermaux iodide-iodate reaction system. Combining their CFD modeling results, the authors suggested that Hartridge–Roughton configuration is an efficient mixing device, while Y-shaped tube presents a poor micromixing performance due to its weak turbulence structure. Similarly, for the purpose of the improvement of micromixing performance in high shear mixer, Qin et al[6] also successfully applied such reaction system combined CFD modeling to show that the single-row blade screen mixer performs better than the dual rows ultrafine-teethed mixer. They attributed this result to the enhanced turbulence intensity, and suggested that further improvement can be realized by the addition of liquid distributors, and the modification of blades. Luo et al[39] proposed a modified geometry to optimize the premixing behavior in the helical tube reactor, and their CFD modeling results were confirmed experimentally by adopting the iodide-iodate reaction system. Due to the significant advantages of the Villermaux iodide-iodate reaction system, it is adopted in the present study to evaluate micromixing performance.

2.1 | Reaction kinetics

The reaction system can be described by three sub-reactions, which are expressed as

$$H_2BO_3^- + H^+ \overset{k_1}{\Leftrightarrow} H_3BO_3 \,(\text{quasi} - \text{instantaneous}) \tag{1}$$

$$5I^- + IO_3^- + 6H^+ \overset{k_2}{\Leftrightarrow} 3I_2 + 3H_2O \,(\text{fast}) \tag{2}$$

$$I_2 + I^- \underset{k'_3}{\overset{k_3}{\rightleftharpoons}} I_3^- \tag{3}$$

where H^+ stands for the hydrogen ion of the sulfuric acid (H_2SO_4). Such a system can be regarded as having a competition between the first neutralization reaction and the second Dushman reaction that produces the by-product of iodine, leading to the occurrence of the third reaction. The concentration of triiodide (I_3^-) in the third reaction can be measured by a UV spectrophotometer. Reaction (1) is quasi-instantaneous with a second-order rate constant k_1 at about $10^{11}\,\text{Lmol}^{-1}\,\text{s}^{-1}$,[40] while Reaction (2) is very fast and has the same order of magnitude as the micromixing process as indicated by Fournier et al.[41] The rate constant k_2 depends on the ionic strength I and will change during the micromixing process,[42] which was found to be well approximated by the following empirical relationships:

$$\log k_2 = 9.28 - 3.66\sqrt{I_i}, I_i < 0.16\,\text{mol}\cdot\text{L}^{-1} \tag{4}$$

$$\log k_2 = 8.38 - 1.51\sqrt{I_i} + 0.23 I_i, I_i > 0.16\,\text{mol}\cdot\text{L}^{-1} \tag{5}$$

The rate laws of Reactions (1) and (2) can be expressed as

$$r_1 = k_1 c_{H_2BO_3^-}\, c_{H^+} \tag{6}$$

$$r_2 = k_2 c_{I^-}^2\, c_{IO_3^-}\, c_{H^+}^2 \tag{7}$$

The equilibrium constant K_3 of Reaction (3) is given by

$$K_3 = \frac{k_3}{k'_3} = \frac{c_{I_3^-}}{c_{I_2} c_{I^-}} \tag{8}$$

For a given reaction, the value of K_3 is only dependent on temperature. For I_3^- formation, K_3 is given by Palmer et al[43] and is expressed as follows:

$$\log K_3 = \frac{555}{T} + 7.355 - 2.575 \log T \tag{9}$$

Due to these three reactions occurring in one system, there is a material balance on each component. On the basis of yield of iodide ion (i.e., I^-), its material balance can be written as

$$c_{I^-} = \frac{V_1 c_{I_0^-}}{V_0 + V_1} - \frac{5}{3}\left(c_{I_3^-} + c_{I_2}\right) - c_{I_3^-} \tag{10}$$

where $c_{I_0^-}$ stands for the initial concentration of I^-. V_0 represents the volume of H_2SO_4 solution, while V_1 is the volume of the mixture

solution of reactants. H_2SO_4, serving as the limiting agent, is additionally injected to the system to trigger the parallel competing reaction between Reactions (1) and (2).

Combining Equations (8) and (9) with Equation (10), the concentration of iodine (I_2) can be calculated from Equation (11).

$$-\frac{5}{3}c_{I_2}^2+\left(\frac{V_1 c_{I_0^-}}{V_0+V_1}-\frac{8}{3}c_{I_3^-}\right)c_{I_2}-\frac{c_{I_3^-}}{K_3}=0 \tag{11}$$

The main by-product of the Villermaux iodide–iodate reaction system is I_2. With the presence of excessive I^-, I_2 will further react with I^- to generate I_3^- until an equilibrium is reached. Since I_3^- has absorption peaks at the wavelength of 288 and 353 nm in the spectrum, the concentration of I_3^- can be measured by a UV spectrophotometer. However, I^- also presents the absorption peak at around 288 nm in the spectrum. In order to reduce interference from the other components, the use of 353 nm as an indicator is preferable for the concentration measurement of I_3^-. According to Beer–Lambert's law, the absorption A of a component across a quartz cell with a thickness Ψ is linearly dependent on its concentration c and molar extinction coefficient e, that is,

$$A_{353}=e_{353}c_{I_3^-}\Psi \tag{12}$$

For a particular product and a quartz cell, the molar extinction coefficient e and thickness Ψ are fixed values. Thus, the absorption is linearly dependents on the concentration of I_3^-. The calibration curve of I_3^- was firstly prepared before experimental work was performed as shown in Figure 1. The calibration curve with R^2 equal to 0.987 highlights that the Beer–Lambert's law is valid within the range of I_3^- concentration chosen in the present study. For the micromixing experiment test, once the absorption of triiodide ion is obtained from the UV spectrophotometer, the concentration of I_3^- can be calculated from the calibration curve.

2.2 | Definition of segregation index

The segregation index (Xs) is defined as the relative amount of H^+ consumed by Reaction (2). For a perfect micromixing condition, all H^+ would be evenly distributed in the system and then immediately consumed by borate ion (i.e., $H_2BO_3^-$) without the appearance of Reaction (2). On the contrary, for poor micromixing, $H_2BO_3^-$ and I^-, iodate ion (i.e., IO_3^-) would compete with H^+ simultaneously. According to stoichiometry, the yield of I_2 from Reaction (2) for a total segregation is expressed as,

$$Y_{ST}=\frac{6n_{IO_{3,0}^-}}{6n_{IO_{3,0}^-}+n_{H_2BO_{3,0}^-}} \tag{13}$$

In practice, I_2 exists in two parts. One is generated in Reaction (2), and the other one is consumed by Reaction (3). Thus, the yield of I_2 should be calculated through the ratio of total mole of both I_2 and IO_3^- to the initial mole of H^+, as defined by

$$Y=\frac{2\left(n_{I_2}+n_{I_3^-}\right)}{n_{H_0^+}} \tag{14}$$

Therefore, *X*s can be written as

$$X_S=\frac{Y}{Y_{ST}}=\frac{n_{I_2}+n_{I_3^-}}{n_{H_0^+}}\left(2+\frac{n_{H_2BO_{3,0}^-}}{3n_{IO_{3,0}^-}}\right) \tag{15}$$

Equation (15) can be converted in terms of the concentration given by Equation (16).

$$X_S=\frac{V_1\left(c_{I_2}+c_{I_3^-}\right)}{n_{H_0^+}}\left(2+\frac{c_{H_2BO_{3,0}^-}}{3c_{IO_{3,0}^-}}\right) \tag{16}$$

By definition, the value of X_S varies between 0 and 1 with a lower value indicating a better micromixing performance.

$X_s = 0$ Perfect micromixing

$X_s = 1$ Total segregation

$0 < X_s < 1$ Partial segregation

2.3 | CFD modeling

In order to get a better understanding of the mixing conditions in the TC reactor, the flow fields of two different inner cylinders were simulated using commercial CFD code, FLUENT 17.0. Based on the structures of the two types of inner cylinder shown in Figure 2, the geometry was created by ANSYS ICEM. Then, the computational domain was divided into two zones, connected by the predefined interface. The total meshes have around 1,100,000 cells, with each direction of 16 × 147 × 480 (radial × circumferential × axial). Our previous work[19] presents the details for such flow field simulation, where RNG k-ε turbulent model was adopted. The boundary conditions were set as velocity inlet and pressure outlet with no slip wall. The discretized equations were realized by the SIMPLEC algorithm. In addition, in order to validate the turbulent model being appropriately

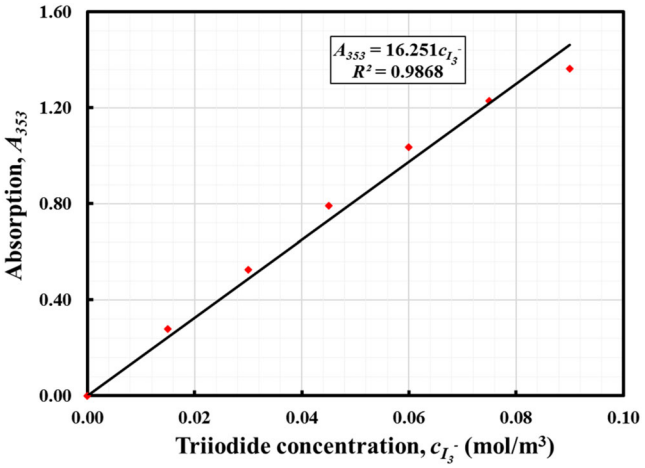

FIGURE 1 Calibration curve of the triiodide ion concentration at 353 nm in the UV spectrum [Color figure can be viewed at wileyonlinelibrary.com]

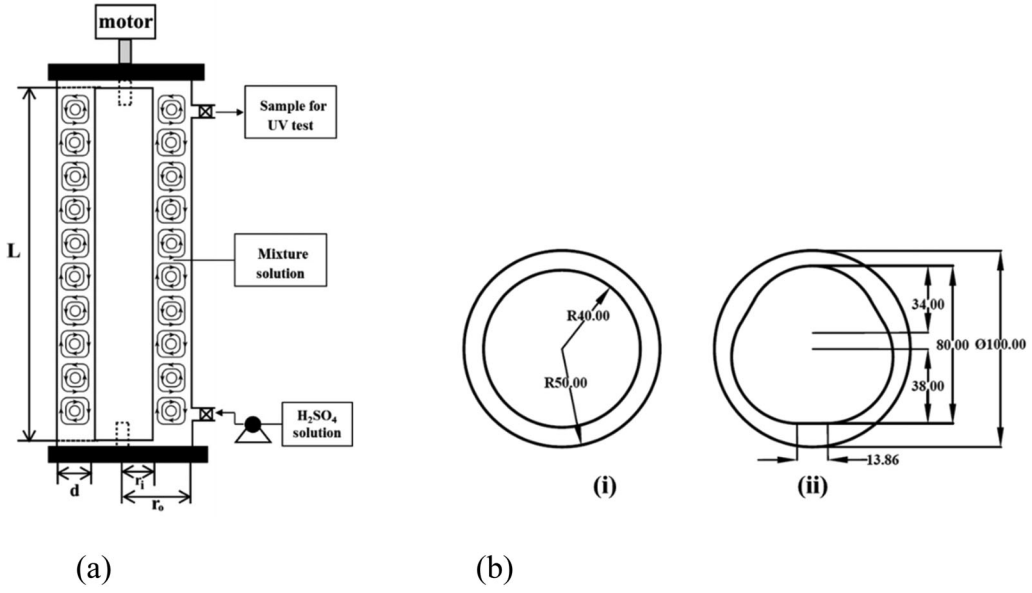

FIGURE 2 (a) Schematic diagram of experimental setup and (b) Schematic of cross-section profiles for the: (i) CTC and (ii) LTC

TABLE 1 Dimensions of the TC reactor

Dimension	CTC	LTC
Reactor length, L (mm)	300.00	300.00
Outer cylinder radius, r_o (mm)	50.00	50.00
Inner cylinder radius (original or equivalent), r_i (mm)	40.00	40.19
Gap size, d (mm)	10.00	9.81

chosen, and major flow features can be captured, model validation has been performed in advance by the comparison with Haut et al's experimental data.[44] The results are shown in Figure S1.

3 | EXPERIMENTAL WORK

3.1 | Apparatus setup

The apparatus of the TC reactor is illustrated in Figure 2(a). Two types of inner cylinder are adopted in this study, one being the classical inner cylinder with a circular cross-sectional profile and the other is a lobed cross-sectional profile inner cylinder, whose cross section consists of three identical arcs connected by three tangential lines. Figure 2(b) displays the cross-sectional profiles for both geometries. Here, the abbreviations of CTC and LTC denote the classical TC reactor and the lobed TC reactor, respectively. The dimensions of the TC reactor are described in Table 1.

In order to determine the flow pattern in the TC reactor, the Reynolds number based on the gap size has been adopted, as defined by

$$Re = \frac{\omega_i r_i d}{\nu} \quad (17)$$

where ω_i and r_i are the angular velocity and the radius of the inner cylinder, respectively. d is the gap size, and ν is the kinematic viscosity of the suspension. In this study, various cases with different Reynolds number have been investigated by changing the rotational speed of the inner cylinder. The critical Reynolds number (Re_c), which indicates the presence of Taylor vortex flow was found to be about 97 with the classical inner circular cylinder (i.e., radius ratio $\eta = \frac{r_i}{r_o} = 0.8$). When the Reynolds number exceeds the critical Reynolds number, the flow pattern will experience a series of instabilities, including wavy Taylor vortex flow and turbulent Taylor vortex flow, which can finally develop into turbulent Taylor flow.[45]

3.2 | Villermaux reaction procedures

All the agents were purchased from Sinopharm Chemical Reagent Co., Ltd of China with a purity level of above 99.0%. The reactor gap was filled with the mixture solution of boric acid (H_3BO_3, 0.089 mol/L), potassium iodide (KI, 0.0116 mol/L), potassium iodate (KIO_3, 0.00233 mol/L), and sodium hydroxide (NaOH) with deionized water. NaOH was used to adjust the pH value around 10.0 in order to prevent the reaction between KI and KIO_3 with the presence of H^+. Therefore, the pH value should be carefully controlled during solution preparation.

The rotational speed was adjusted within the range of 501,000 rpm, corresponding to the Reynolds Number varying from 2000 to 42,000. After the system reached a steady state, H_2SO_4 solution was injected into the reactor from the bottom inlet. In each run, about 3 mL of sample solution was collected for the UV test from the top outlet after completing the mixing. The absorption intensity test was conducted immediately using the UV spectrophotometer (UNICO SQ4802 UV/VIS Spectrophotometer, USA) at the wavelength of

TABLE 2 Operating conditions

Experimental number	Feeding time (s)	H^+ concentration (mol/L)	Rotational speed (rpm)	Reynolds number
R1	120	2.0	50	2094
R2	120	2.0	100	4188
R3	120	2.0	200	8376
R4	120	2.0	300	12564
R5	120	2.0	400	16752
R6	120	2.0	600	25128
R7	120	2.0	800	33504
R8	120	2.0	1000	41880
R9	20	2.0	300	12564
R10	40	2.0	300	12564
R11	60	2.0	300	12564
R12	240	2.0	300	12564
R13	360	2.0	300	12564
R14	480	2.0	300	12564
R15	120	1.2	300	12564
R16	120	1.6	300	12564
R17	120	4.0	300	12564
R18	120	5.0	300	12564
R19	120	6.0	300	12564

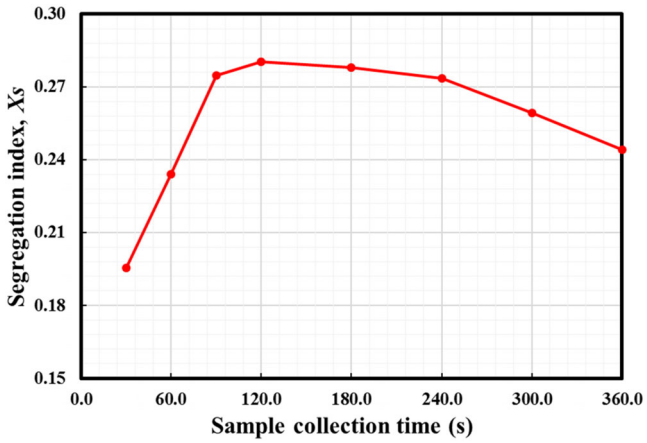

FIGURE 3 Preliminary test of the selection of sample collection time [Color figure can be viewed at wileyonlinelibrary.com]

353 nm to ensure the stability of I_3^-. The experiment and the sample measurement were carried out at the room temperature of 25°C. The operating conditions for both the CTC and LTC are summarized in Table 2.

4 | RESULTS AND DISCUSSION

In the segregation experiments, the sampling location was set with a distance away from the inlet of acid injection. In order to guarantee that a well-established micromixing process is achieved throughout the whole reactor, the collection time after acid injection should be determined in advance. The preliminary experiment was performed at a Reynolds number of 12,564 in the CTC. It can be seen from Figure 3 that the critical collection time is 120 s after finishing the injection of acid. However, within the range from 90 to 240 s, the results used to determine the collection time also appear to be acceptable. One can argue that if the collection time is too short, the macromixing has not been fully achieved, thus resulting in little amount of the product being detected at the outlet. On the other hand, if the collection time is too long, the UV result may lose its accuracy since I_3^- is very sensitive to light. Therefore, the determination of the critical collection time is crucial for acquiring reliable results. It should be noted that for different operating conditions, the critical collection time may be different within the acceptable range. The following discussion on the micromixing in the TC reactor will be based on the samples collected at the critical collection time determined.

4.1 | Effect of feeding time on *Xs*

Mixing in the TC reactor involves all the scales from macro-scale, meso-scale to micro-scale. In order to better separate the influence of macromixing on micromixing and only observe the micromixing behavior, the feeding rate of acid solution should be controlled as low as possible as mentioned earlier. In our experiment, the injection of acid solution was maintained at a constant feeding rate, which means the feeding time should be controlled long enough.

Figure 4 shows the change of *Xs* with feeding time in the CTC and LTC, where *Xs* gradually decreases and reaches an almost constant value with little fluctuation. When taking a very fast injection, the value of *Xs* will be jointly controlled by both macro- and micromixing. Under such a condition, the local concentration gradient can be very high, as the acid plume cannot be dispersed well throughout the whole reactor scale.[1] Accordingly, this will lead to the local excess of H^+ and a large value of *Xs*. However, this is mainly caused by poor dispersion rather than poor micromixing in the reactor, as the effect of macromixing is not eliminated. On the other hand, a fast injection leading to a random fluctuation will break the steady state of flow field. When more turbulent eddies are involved, the dynamic balance of acid engulfment with bulk reactants cannot be achieved. As local $H_2BO_3^-$ is not enough to consume a large amount of H^+, the excessive H^+ will react with I^- and IO_3^-, yielding a large value of *Xs*. With a slow injection of acid, the turbulence is less affected such that the acid has enough time to be dispersed evenly in a macro-scale throughout the reactor and a well-established environment for micromixing is obtained. Consequently, the UV measurement result given by chemical test reactions is free from the macromixing influence and is only dependent on the micromixing behavior. Thus, the feeding time of 120 s was chosen for all the subsequent experiments.

4.2 | Effect of H^+ concentration on *Xs*

Because the linear relationship between I_3^- concentration and its absorption is valid within a particular range, the H^+ concentration should be selected appropriately to avoid excessive or too little I_2 being generated. A wide range of H^+ concentration from 1.2 to 6.0 mol/L has been tested. The experiment was conducted under the condition of the Reynolds number of 12,564 with 1.0 ml injection. It can be seen from Figure 5 that the value of *Xs* firstly increases, then levels off with the increase of H^+ concentration. At a higher H^+ concentration, more time is needed for $H_2BO_3^-$ to neutralize H^+. However, the amount of $H_2BO_3^-$ was kept at a constant level when changing the H^+ concentration. Thus, the excessive H^+ will lead to the occurrence of Reaction (2). It can be seen from the rate laws of Equations (6) and (7) that Reaction (2) is more sensitive to H^+ due to its higher rate order. Moreover, the chemical reaction rate of Reaction (2) is usually higher when compared to the micromixing rate,[41] which will be presented and discussed in Section 4.4. Thus, excessive H^+ leads to the generation of a large amount of I_2, and a high value of *Xs*. It is worth mentioning that the continuous increase of H^+ concentration does not give rise to the continuous increase of *Xs*. Due to the local excess of H^+ concentration, both Reactions (1) and (2) have been completed, which means that all reactants have achieved their maximum conversion. As a result, I_2 concentration will not increase any further. The most sensitive point for the UV detection corresponds to the H^+ concentration of 2.0 mol/L as indicated in Figure 5. This value has been chosen for all the subsequent experiments.

One can see from Figure 5 that micromixing performance in the LTC is better than that of the CTC at all ranges of the H^+ concentration, but such a difference is less noticeable at high H^+ concentration. For the LTC, the rotational lobed inner cylinder generates a periodic variation of the gap size. The circumferential flow will experience an expansion and contraction, leading to the generation of the induced turbulent eddies from the surface of the concaved top of the inner cylinder and the enhanced turbulent eddy interactions. Such turbulent eddy interaction can effectively re-disperse the concentration field of reactants, promoting a better distribution of the reactants, less local H^+ accumulation and less local formation of I_2. This is another piece of evidence to suggest that lobed geometry can effectively reduce the overall mixing time and improve the micromixing efficiency for the TC reactor.

4.3 | Effect of Reynolds number on *Xs*

Figure 6(a) shows the effect of the variation of Reynolds number on *Xs* under the condition of 1.0 ml sulfuric acid solution injected within

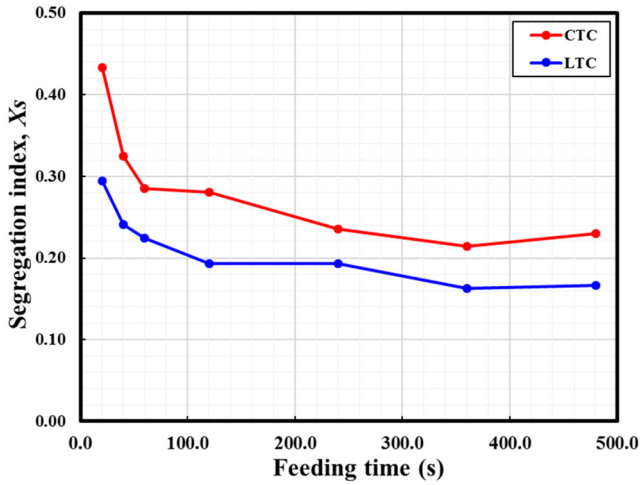

FIGURE 4 Effect of feeding time on segregation index [Color figure can be viewed at wileyonlinelibrary.com]

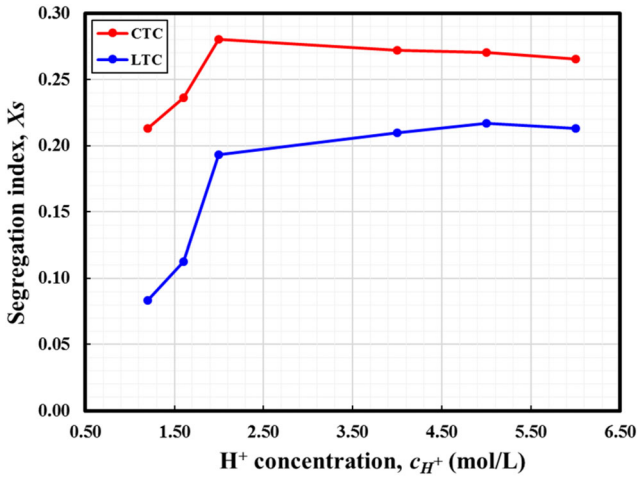

FIGURE 5 Effect of H^+ concentration on segregation index [Color figure can be viewed at wileyonlinelibrary.com]

120 s. With the increase of Reynolds number, *Xs* decreases in both the CTC and LTC. When Reynolds number is greater than 25,128 (corresponding to 600 rpm), the decrease in *Xs* becomes small. At a low rotational speed, that is, a small Reynolds number, *Xs* presents a very high value, and the difference between the CTC and LTC is very small, which can be attributed to the excessive turbulence generated by the lobed inner cylinder being still small. Although the geometry modification can enhance the micromixing to some extent, flow pattern has not become fully turbulent for both the CTC and LTC. The degree of the occurrence of the micromixing may still rely on the molecule-scaled diffusion. The reactant fluid elements that contribute to the micromixing still hold a relatively large size compared with the molecular diffusion length scale. In such case, the micromixing may not be sufficient. With the increase of Reynolds number, turbulence intensity is gradually built up and the flow in the reactor develops to the turbulent state, and the micromixing improves evidenced by drop in *Xs*. Although the chemical reaction occurs at molecular level, the intensified turbulence can provide the environment for reactant fluid elements to break into much smaller size eddies with the surface area for the mass transfer being increased. As a result, mixing diffusion improves and the micromixing rate can be accelerated. Finally, as Reynolds number exceeds 25,128, it is observed that *Xs* levels off, reaching a minimum of about 0.15 and 0.08 for the CTC and LTC, respectively.

We cautiously mention here that the difference of *Xs* between the CTC and LTC becomes remarkable with the flow in the TC reactor to be judged to be fully turbulent. The LTC shows a much better micromixing than the CTC. This may be explained by the facts: First, with the rotation of the inner cylinder, gap size of the LTC varies periodically so that the formed Taylor vortices change and the vortices are deformed. Consequently, this type of perturbation due to the deformation Taylor vortices will induce the generation of small turbulent eddies down to the scales beneficial to the micromixing. Second, Liu et al[19] have compared the turbulent flows generated by the CTL and LTC and shown that the impinging jet region existing between the two toroidal counter-rotating Taylor vortices induces a stronger outward shear gradient in the LTC than that in CTL when the same rotational speed was taken. Thus, it can be claimed that the reactant micro elements entrapped by the turbulent eddies generated by the impinging jet flow shear in the LTC can have a shorter entrainment time than the CTC.

In order to quantitatively describe how *Xs* changes with the Reynolds number, the following relation is proposed, given by

$$Xs = CRe^{b-e-f} \tag{18}$$

where *e* is defined as the eccentricity, shown in Figure S2. The eccentricity defined here is used to involve the effect of geometry modification on micromixing. From the definition of Reynolds number in Equation (17), it can be seen that both CTC and LTC were operated at the identical global turbulent condition. However, the LTC shows an improved micromixing performance. Thus, it can be deduced that there is an additional local turbulent effect on micromixing due to geometry modification. As *Xs* shows a negative relationship with Reynolds number, a negative eccentricity is introduced to the power of Reynolds number. By definition, the eccentricity for the CTC is equal to 0, for the LTC equal to 0.2. Thus, Equation (18) can be converted into $Xs = C' Re^{b} \cdot DRe^{-0.2-f}$, where Re^{-f} can be seen as the additional effect, which needs further investigation. By taking the logarithmic transformation of both sides, a liner relationship is obtained. Using this regression fitting, it was found that well fitted relation for the CTC is $lnXs = -0.451lnRe + 2.963$ with $R^2 = 0.968$ and the same fitted relation for the LTC is $lnXs = -0.635lnRe + 4.319$ with $R^2 = 0.986$, respectively. For the LTC, the fitted relation can be further converted into $lnXs = (-0.451lnRe + 2.963) - 0.2lnRe + (0.016lnRe + 1.35)$ to separate the effect of geometry modification (i.e., $-0.2lnRe$). The additional positive term, $0.016lnRe + 1.35$ may be caused by suppression on turbulence, such as wall friction.

Turbulence intensity is suggested to have a strong relationship with micromixing performance by Qin et al.[6] It is defined as

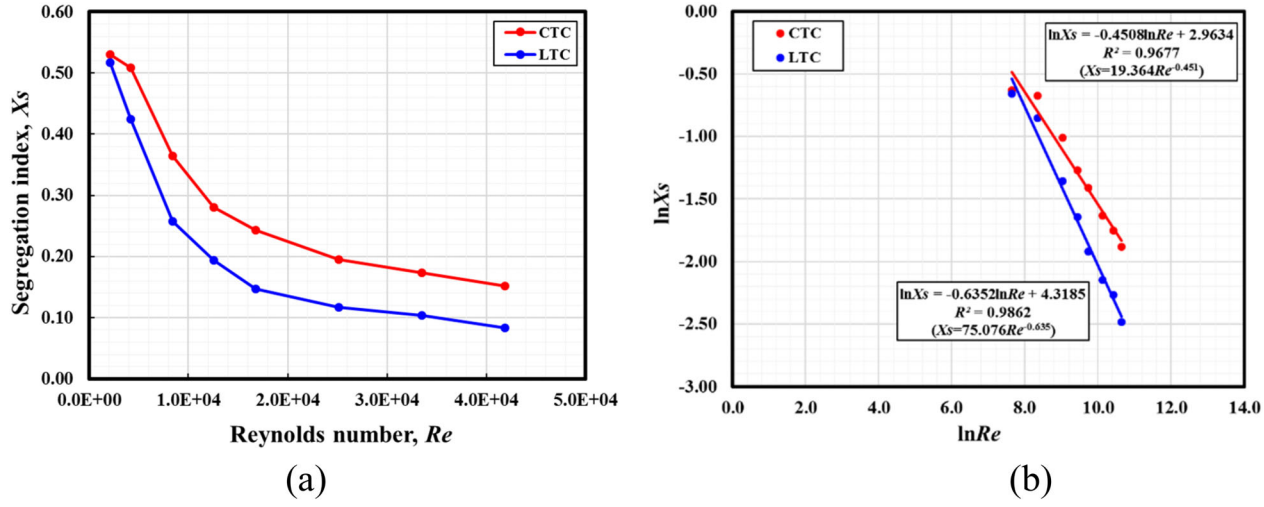

FIGURE 6 (a) Effect of Reynolds number on segregation index and (b) Segregation index as a function of Reynolds number [Color figure can be viewed at wileyonlinelibrary.com]

the ratio of velocity fluctuation to mean flow velocity, expressed as

$$I = \frac{u'}{u_{\text{mean}}} \tag{19}$$

where u' is the velocity fluctuation, and u_{mean} is the velocity of the mean flow. Turbulence intensity measured on the surface of the inner cylinder for both the CTC and LTC based on CFD simulation is shown in Figure 7. For three representative rotational speeds, 100, 600, and 1000 rpm, the corresponding Reynolds numbers are 4188, 25,128, and 41,880, respectively. It can be seen clearly from the figure that the turbulence intensity is enhanced with the increase of Reynolds number for both the CTC and LTC but the enhancement for the LTC is significantly larger than that in the CTC. Also, the highest turbulence intensity appears at regions of three concaved arcs, corresponding to the smallest gap regions in the LTC. As the Reynolds number for the CTC and LTC is the same, it cannot involve the effect of geometry modification. In order to show the effect of hydrodynamic heterogeneity on micromixing, the correlation between the turbulence intensity and $1/Xs$ is proposed.

$$R_{IXs} = <I> \frac{1}{X_s} \tag{20}$$

$$<I> = \frac{1}{V}\int_0^V I dV \tag{21}$$

where <*I*> is the volume averaged turbulence intensity. Figure 8 shows such correlation. Greater values often indicate a strong coupling between two variables at some given conditions (i.e., Reynolds number). On one hand, the correlation value increases with the increase of Reynolds number, indicating a positive correlation between turbulence intensity and micromixing performance. On the other hand, the difference between the LTC and CTC is getting significant with the increase of Reynolds number, which indicates that at high Reynolds number, turbulence in the LTC has an enhanced effect on micromixing. This can be attributed to the modification of the inner cylinder configuration of the TC reactor. As the CTC and LTC were operated at the identical Reynolds number, the only difference between the both lies in the cross-sectional profile of the inner cylinder. Due to the periodic variation of gap size in the LTC, Taylor vortices will be deformed, and more turbulent eddies can be generated, thus creating local homogenous environment for micromixing. This can be confirmed by observing energy dissipation rate, provided in Figure S3. As small eddies will be eventually dissipated, more energy consumption often indicates more turbulent eddies generated. Generally, small eddies down to the Kolmogorov scale are recognized to be isotropic. Therefore, micromixing occurring in such environment will demonstrate good performance.

4.4 | Characterization of micromixing time

In order to compare the micromixing efficiency of the adopted TC reactor especially the lobed inner cylinder with conventional stirred tank, the micromixing times for different reactors are evaluated. Many models have been proposed to estimate micromixing time. Among these models, the IEM model,[46] the EDD model,[47] the E-model,[48] and the incorporation model[29] are representatives. However, the incorporation model has been widely used and recognized as illustrated in Figure 9. This model assumes that the limited agent, acid occupying Environment 2, is divided into several aggregates, which then are progressively invaded by surrounding solution from Environment 1. Consequently, the volume of acid aggregates gradually grows due to the incorporation, based on $V_2 = V_{20}g(t)$. The characteristic incorporation time is assumed to be equivalent to the micromixing time. Fournier et al[41] proposed a dilution-reaction equation in the reaction Environment 2, which is found to be suitable for the description of the present employed TC reactor system, given by

$$\frac{dc_j}{dt} = (c_{j10} - c_j)\frac{1}{g}\frac{dg}{dt} + r_j \tag{22}$$

where c_j is the reactant concentration, and species j denotes $H_2BO_3^-$, H^+, I^-, IO_3^-, I_2, and I_3^-. c_{j10} is the concentration of surrounding solution

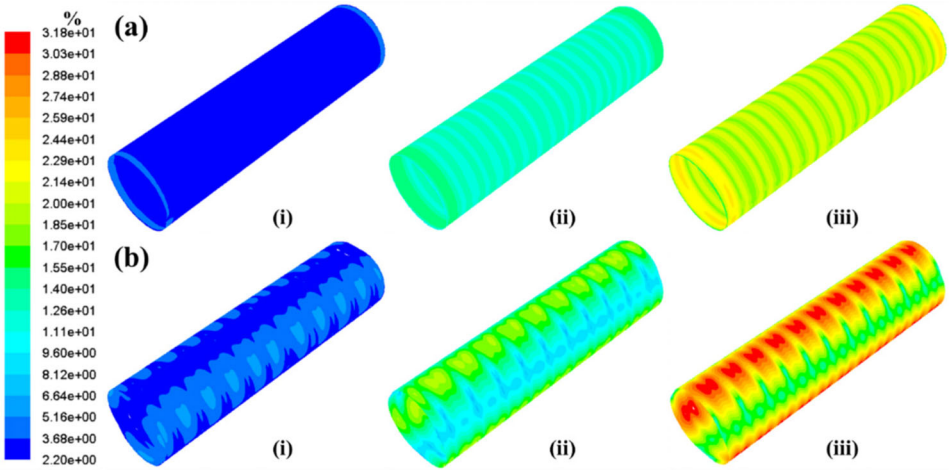

FIGURE 7 Distribution of the turbulent intensity on the surface of the inner cylinder: (a) CTC; and (b) LTC at different Reynolds numbers: (i) 4188; (ii) 25,128 and (iii) 41,880 [Color figure can be viewed at wileyonlinelibrary.com]

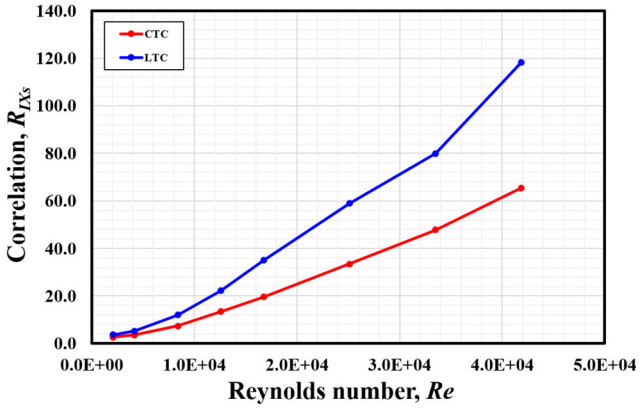

FIGURE 8 Correlation between the turbulence intensity and segregation index at different Reynolds numbers [Color figure can be viewed at wileyonlinelibrary.com]

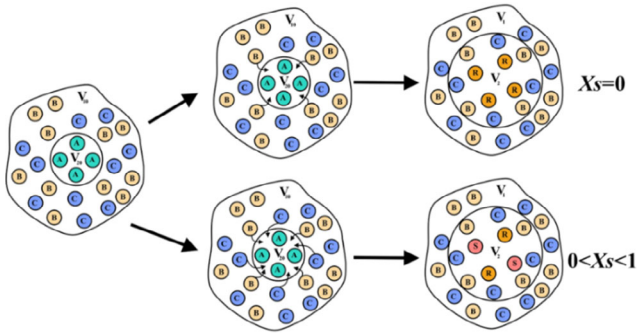

FIGURE 9 Principle of micromixing process based on the incorporation model [Color figure can be viewed at wileyonlinelibrary.com]

(i.e., the initial concentration of species j in Environment 1). r_j is the net production rate of species j, and g denotes the mass exchange rate between reactant fluid particle and its surrounding solution. A large value of dg/dt indicates a fast dilution, indicating a good mixing performance between the feeding acid and its surrounding solution. The empirical equation of the growing law for acid aggregates can be expressed as an exponential function of micromixing time, t_m, which reads

$$g(t) = \exp\left(\frac{t}{t_m}\right) \tag{23}$$

Thus, Equation (22) can be converted into the following form,

$$\frac{dc_j}{dt} = \frac{c_{j10} - c_j}{t_m} + r_j \tag{24}$$

From Equation (24), the mass balance equation of individual species can be obtained. In total, there are six transport equations to be solved. In order to reduce computational cost, the W-Z transformation was adopted to reduce the number of solutions and the simplification yields

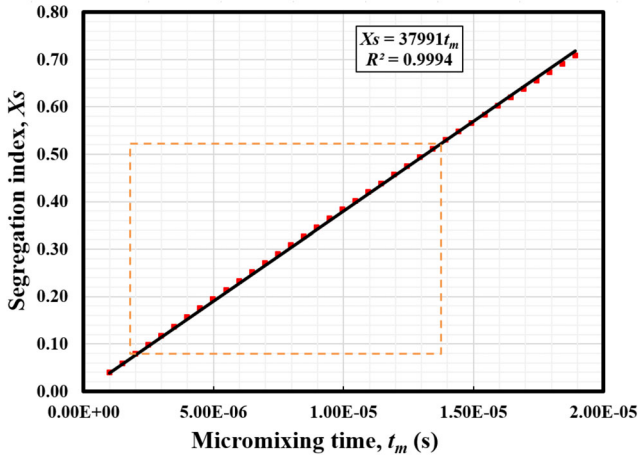

FIGURE 10 Predicted segregation index and micromixing time based on the incorporation model [Color figure can be viewed at wileyonlinelibrary.com]

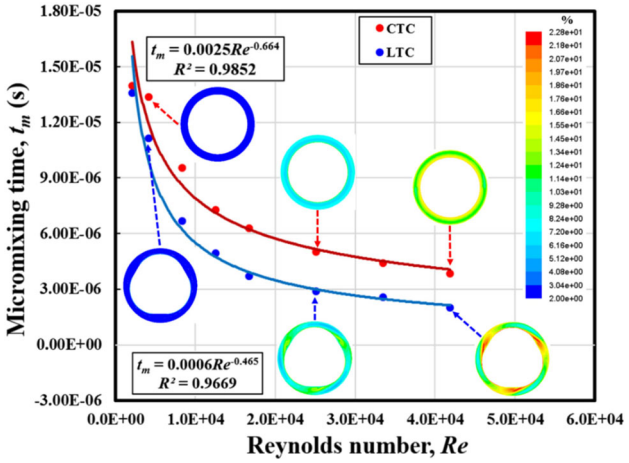

FIGURE 11 Micromixing time as a function of Reynolds number [Color figure can be viewed at wileyonlinelibrary.com]

$$\frac{dW}{dt} = -\frac{c_{H_2BO_3^-,10} + W}{t_m} - 6r_2 \tag{25}$$

$$\frac{dY}{dt} = \frac{c_{I^-,10} - Y}{t_m} - 8r_2 \tag{26}$$

$$\frac{dZ}{dt} = \frac{c_{I^-,10} - Z}{t_m} - 5r_2 \tag{27}$$

$$\frac{dc_{IO_3^-}}{dt} = \frac{c_{IO_3^-,10} - c_{IO_3^-}}{t_m} - r_2 \tag{28}$$

where $W = c_{H^+} - c_{H_2BO_3^-}$, $Y = c_{I^-} - c_{I_2}$, and $Z = c_{I^-} + c_{I_3^-}$. Equations (25)–(28) can be solved numerically by iteration, where the initial conditions are given by $W = c_{H^+,0}$, $Y = 0$, $Z = 0$, and $c_{IO_3^-} = 0$. The iteration ends as H^+ concentration approaches 0. Acid concentration reaches its highest value at the inlet, then, it disperses within a very limited range and is consumed quickly. Thus, H^+ concentration is assumed to

be at its initial value, $c_{H^+,0}$ during the iteration before it is completely consumed. The forth-order Runge–Kutta method was adopted in the present study to calculate species concentration. First, a series value of t_m is assumed. Following the Runge–Kutta iteration, Equations (25)–(28) are solved, and the concentrations of individual species are obtained. Subsequently, a set of segregation index *X*s can be calculated based on Equation (16). Figure 10 depicts the obtained relation of *X*s against the micromixing time t_m (*X*s = 37, 991 t_m). This relation can be used to evaluate the micromixing time in TC reactor based on the value of *Xs* obtained from the experimental results, which are marked in Figure 10. Figure 11 shows the relationship between the Reynolds number and micromixing time in the CTC and LTC. For better description, the contour of turbulent intensities in the circumferential direction for both the CTC and LTC is also shown in Figure 11, where the intensified regions by geometry modification can be seen clearly. By using power law fitting, the micromixing time for both the CTC and LTC can be approximated by $t_m = 0.0025Re^{-0.664}$ and $t_m = 0.0006Re^{-0.456}$, respectively.

Damköhler number (*Da*), defined as the ratio of the chemical reaction timescale (reaction rate) to the mixing timescale (mixing rate), is also used to characterize the impact of hydrodynamics in the TC reactor on chemical reaction. Here, we use the obtained relations for the micromixing time to estimate Da_1 and Da_2 for Reactions (1) and (2), respectively. The chemical reaction time for Reactions (1) and (2) is given by

$$t_{r_1} = \frac{\min\left(c_{H_2BO_3^-,0}; c_{H^+,0}\right)}{r_1} \tag{29}$$

$$t_{r_1} = \frac{\min\left(\frac{3}{5}c_{I^-,0}; 3c_{IO_3^-,0}; \frac{1}{2}c_{H^+,0}\right)}{r_2} \tag{30}$$

Thus, Da_1 and Da_2 can be estimated using Equations (31) and (32).

$$Da_1 = \frac{t_m}{t_{r_1}} = t_m k_1 c_{H^+,0} \tag{31}$$

$$Da_2 = \frac{t_m}{t_{r_2}} = t_m k_2 c_{I^-,0}^2 c_{H^+,0}^2 \tag{32}$$

The estimated $Da_1 = 4.2 \times 10^5$–2.8×10^6 is much great than 1, indicating that Reaction (1) is an instantaneous reaction. $Da_2 = 3.2 \times 10^{-3}$–$2 \times 10^{-2}$ has the order of 10^{-2}, which is small than 1. Both results indicate that the iodide-iodate reaction system used for evaluation of the micromixing performance in the TC reactor to be suitable.

Compared with the conventional stirred tank reactor, in which the micromixing time is the order of 20 ms,[41] the order of micromixing time in the TC reactor is evaluated to be 10^{-5} s based on the above discussion. It thus can be claimed that the TC reactor can have a better micromixing performance than the traditional stirred tank reactor as far as those fast chemical processes controlled by the mixing are concerned. The use of the lobed inner cylinder configuration in the TC reactor can further shorten the micromixing time due to the local turbulence intensification.

5 | CONCLUSIONS

The micromixing performance in a TC reactor with two different inner cylinder geometries has been evaluated based on the parallel competing iodide-iodate reaction system to characterize the impact of the inner cylinder configuration variations, which will significantly affect the micromixing process by changing hydrodynamic environment. Segregation index *X*s was employed as an indicator to characterize the micromixing efficiency. In order to assess the effects of various factors, the sample collection time has been carefully determined to ensure the reliable UV results. The acid concentration was also carefully chosen to avoid over-loading, while the injection of acid was controlled to keep the feeding as slow as possible in order to eliminate the impact of macromixing in the TC reactor. The conclusions reached for the present study can be summarized as follows:

1. The segregation experimental results have indicated that the value of *X*s decreases with the increase of Reynolds number for both inner cylinder configurations but the LTC exhibits a better micromixing performance than the CTC as *X*s for the LTC is smaller than the CTC.
2. CFD simulation results have revealed that the turbulence intensity generated in the jet regions in vicinity of the inner cylinder in the LTC is stronger than that in the CTC, which subsequently enhances the local micromixing. This clearly indicates that the modification of the inner cylinder configuration (here, the use of a lobed cross-sectional profile) may improve the micromixing behavior significantly.
3. Predictions made by employing the incorporation model show that the micromixing time is estimated to be of the order of 10^{-5} s for the TC reactor, much smaller than that of the traditional stirred tank reactor according to the open literature. In addition, the LTC shows a shorter micromixing time than the CTC.

ACKNOWLEDGMENT

This work was carried out at the International Doctoral Innovation Centre (IDIC), UNNC. The authors acknowledge the financial support by National Natural Science Foundation of China (NSFC) through the grant (Nos. 21761132026, 21576141, 21606259). The authors also would like to thank the reviewers for their expert guidance on revising the manuscript of this article.

DATA AVAILABILITY STATEMENT

The data that support the findings of this study are available from the corresponding author upon reasonable request.

NOMENCLATURE

A_{353}	absorption at 353 nm
c_j	concentration of species *j*, mol/L
d	gap width, m
Da	Damköhler number
e	eccentricity
e_{353}	molar extinction coefficient, L/mol/mm

g	growing rate for incorporation model
I	turbulent intensity, %
I_i	ionic strength, mol/L
k	reaction rate constant, m^2/s^2, dimension dependent on reaction order
K_3	equilibrium constant for Reaction (3)
L	reactor length, m
n_j	mole of species j, mol
r	chemical reaction rate, mol/L/s
r_i	radius of the inner cylinder, m
r_o	radius of the lobed outer cylinder, m
Re	Reynolds number
R_{IXs}	correlation
t_m	micromixing time, s
t_r	chemical reaction time, s
T	thermodynamic temperature, K
Xs	segregation index
Y	yield of iodine

GREEK LETTERS

ν	kinematic viscosity of the fluid, m^2/s
ω_i	rotational speed of the inner cylinder, rad/s
Ψ	thickness of quartz cell, mm

ORCID

Xiaogang Yang https://orcid.org/0000-0002-0630-5193

REFERENCES

1. Baldyga J. Mixing and fluid dynamics effects in particle precipitation processes. *KONA Powder Particle J*. 2016;33:127-149.
2. Jacobsen NC, Hinrichsen O. Micromixing efficiency of a spinning disk reactor. *Ind Eng Chem Res*. 2012;51(36):11643-11652.
3. Liu Z, Guo L, Huang T, Wen L, Chen J. Experimental and CFD studies on the intensified micromixing performance of micro-impinging stream reactors built from commercial T-junctions. *Chem Eng Sci*. 2014;119:124-133.
4. Shi X, Xiang Y, Wen LX, Chen JF. CFD analysis of flow patterns and micromixing efficiency in a Y-type microchannel reactor. *Ind Eng Chem Res*. 2012;51(43):13944-13952.
5. Gao Z, Han J, Bao Y, Li Z. Micromixing efficiency in a T-shaped confined impinging jet reactor. *Chin J Chem Eng*. 2015;23(2):350-355.
6. Qin H, Zhang C, Xu Q, et al. Geometrical improvement of inline high shear mixers to intensify micromixing performance. *Chem Eng J*. 2017;319:307-320.
7. Jung WM, Kang SH, Kim WS, Choi CK. Particle morphology of calcium carbonate precipitated by gas–liquid reaction in a Couette–Taylor reactor. *Chem Eng Sci*. 2000;55(4):733-747.
8. Tang Z, Kim WS, Yu T. Studies on morphology changes of copper sulfide nanoparticles in a continuous Couette-Taylor reactor. *Chem Eng J*. 2019;359:1436-1441.
9. Mayra QP, Kim WS. Agglomeration of Ni-Rich hydroxide in reaction crystallization: Effect of Taylor vortex dimension and intensity. *Cryst Growth Des*. 2015;15(4):1726-1734.
10. Thai DK, Mayra QP, Kim WS. Agglomeration of Ni-rich hydroxide crystals in Taylor vortex flow. *Powder Technol*. 2015;274:5-13.
11. Kim JE, Kim WS. Synthesis of core–shell particles of nickel–manganese–cobalt hydroxides in a continuous Couette-Taylor crystallizer. *Cryst Growth Des*. 2017;17(7):3677-3686.
12. Aljishi MF, Ruo AC, Park JH, Nasser B, Kim WS, Joo YL. Effect of flow structure at the onset of instability on barium sulfate precipitation in Taylor–Couette crystallizers. *J Cryst Growth*. 2013;373:20-31.
13. Park S, Kim WS. Influence of fluid motions on polymorphic crystallization of L-histidine: Taylor vortex flow and turbulent Eddy flow. *Cryst Growth Des*. 2018;18(2):710-722.
14. Nguyen AT, Kim JM, Chang SM, Kim WS. Phase transformation of guanosine 5-monophosphate in continuous Couette-Taylor crystallizer: experiments and numerical modeling for kinetics. *Ind Eng Chem Res*. 2011;50(6):3483-3493.
15. Zhu Q, Xiao H, Zhang R, Geng S, Huang Q. Effect of impeller type on preparing spherical and dense $Ni_{1-x-y}Co_xMn_y(OH)_2$ precursor via continuous co-precipitation in pilot scale: A case of $Ni_{0.6}Co_{0.2}Mn_{0.2}(OH)_2$. *Electrochim Acta*. 2019;318:1-3.
16. Soos M, Wu H, Morbidelli M. Taylor-Couette unit with a lobed inner cylinder cross section. *AIChE J*. 2007;53(5):1109-1120.
17. Li G, Yang X, Ye H. CFD simulation of shear flow and mixing in a Taylor–Couette reactor with variable cross-section inner cylinders. *Powder Technol*. 2015;280:53-66.
18. Ehrl L, Soos M, Wu H, Morbidelli M. Effect of flow field heterogeneity in coagulators on aggregate size and structure. *AIChE J*. 2010;56(10):2573-2587.
19. Liu L, Yang X, Li G, Huang X, Xue C. Shear controllable synthesis of barium sulfate particles using lobed inner cylinder Taylor-Couette flow reactor. *Adv Powder Technol*. 2020;31(3):1088-1099.
20. Santiago PA, de Campos GR, Suazo CA. Performance of a vortex flow bioreactor for cultivation of CHO-K1 cells on microcarriers. *Process Biochem*. 2011;46(1):35-45.
21. Desmet G, Verelst H, Baron GV. Local and global dispersion effects in Couette-Taylor flow—II. Quantitative measurements and discussion of the reactor performance. *Chem Eng Sci*. 1996;51(8):1299-1309.
22. Sorg R, Tanzeglock T, Soos M, et al. Minimizing hydrodynamic stress in mammalian cell culture through the lobed Taylor-Couette bioreactor. *Biotechnol J*. 2011;6(12):1504-1515.
23. Drozdov SM. A numerical investigation of a modified Couette-Taylor apparatus with application to industrial mixing. *Theor Comp Fluid Dyn*. 2002;16(1):17-28.
24. Racina A, Kind M. Specific power input and local micromixing times in turbulent Taylor–Couette flow. *Exp Fluids*. 2006;41(3):513-522.
25. Richter O, Hoffmann H, Kraushaar-Czarnetzki B. Effect of the rotor shape on the mixing characteristics of a continuous flow Taylor-vortex reactor. *Chem Eng Sci*. 2008;63(13):3504-3513.
26. DiPrima RC, Eagles PM, Ng BS. The effect of radius ratio on the stability of Couette flow and Taylor vortex flow. *Phys Fluids*. 1984;27(10):2403-2411.
27. Xiao Q, Lim TT, Chew YT. Second Taylor vortex flow: effects of radius ratio and aspect ratio. *Phys Fluids*. 2002;14(4):1537-1539.
28. Richter O, Menges M, Kraushaar-Czarnetzki B. Investigation of mixing in a rotor shape modified Taylor-vortex reactor by the means of a chemical test reaction. *Chem Eng Sci*. 2009;64(10):2384-2391.
29. Villermaux J, Falk L, Fournier MC. Potential use of a new parallel reaction system to characterize micromixing in stirred reactors. *AIChE Symp Ser*. 1994;90(299):50-54.
30. Fournier MC, Falk L, Villermaux J. A new parallel competing reaction system for assessing micromixing efficiency—experimental approach. *Chem Eng Sci*. 1996;51(22):5053-5064.
31. Bourne JR. Mixing effects during the bromination of 1,3,5-trimethoxybenzene. *Chem Eng Sci*. 1977;32(12):1538-1539.
32. Bourne JR, Kozicki F, Rys P. Mixing and fast chemical reaction—I: Test reactions to determine segregation. *Chem Eng Sci*. 1981;36(10):1643-1648.

33. Bourne JR, Rohani S. Micro-mixing and the selective iodination of l-tyrosine. *Chem Eng Res Des*. 1983;61(5):297-302.
34. Villermaux J, Falk L. A generalized mixing model for initial contacting of reactive fluids. *Chem Eng Sci*. 1994;49(24):5127-5140.
35. Habchi C, Della Valle D, Lemenand T, et al. A new adaptive procedure for using chemical probes to characterize mixing. *Chem Eng Sci*. 2011;66(15):3540-3550.
36. Luo JZ, Luo Y, Chu GW, et al. Micromixing efficiency of a novel helical tube reactor: CFD prediction and experimental characterization. *Chem Eng Sci*. 2016;155:386-396.
37. Lemenand T, Della Valle D, Habchi C, Peerhossaini H. Micro-mixing measurement by chemical probe in homogeneous and isotropic turbulence. *Chem Eng J*. 2017;314:453-465.
38. Bertrand M, Lamarque N, Lebaigue O, Plasari E, Ducros F. Micromixing characterisation in rapid mixing devices by chemical methods and LES modelling. *Chem Eng J*. 2016;283:462-475.
39. Luo JZ, Chu GW, Luo Y, Arowo M, Sun BC, Chen JF. Regulating the micromixing efficiency of a novel helical tube reactor by premixing behavior optimization. *AIChE J*. 2017;63(7):2876-2887.
40. Unadkat H, Nagy ZK, Rielly CD. Investigation of turbulence modulation in solid–liquid suspensions using parallel competing reactions as probes for micro-mixing efficiency. *Chem Eng Res Design*. 2013;91(11):2179-2189.
41. Fournier MC, Falk L, Villermaux J. A new parallel competing reaction system for assessing micromixing efficiency—determination of micromixing time by a simple mixing model. *Chem Eng Sci*. 1996;51(23):5187-5192.
42. Guichardon P, Falk L. Characterisation of micromixing efficiency by the iodide–iodate reaction system. Part I: experimental procedure. *Chem Eng Sci*. 2000;55(19):4233-4243.
43. Palmer DA, Ramette RW, Mesmer RE. Triiodide ion formation equilibrium and activity coefficients in aqueous solution. *J Solution Chem*. 1984;13(9):673-683.
44. Haut B, Amor HB, Coulon L, Jacquet A, Halloin V. Hydrodynamics and mass transfer in a Couette–Taylor bioreactor for the culture of animal cells. *Chem Eng Sci*. 2003;58(3–6):777-784.
45. Grossmann S, Lohse D, Sun C. High–reynolds number taylor-couette turbulence. *Annu Rev Fluid Mech*. 2016;48:53-80.
46. Costa P, Trevissoi C. Reactions with non-linear kinetics in partially segregated fluids. *Chem Eng Sci*. 1972;27(11):2041-2054.
47. Baldyga J, Bourne JR. A fluid mechanical approach to turbulent mixing and chemical reaction part II micromixing in the light of turbulence theory. *Chem Eng Commun*. 1984;28(4–6):243-258.
48. Baldyga J, Bourne JR. Simplification of micromixing calculations. I. Derivation and application of new model. *Chem Eng J*. 1989;42(2):83-92.

SUPPORTING INFORMATION

Additional supporting information may be found online in the Supporting Information section at the end of this article.

How to cite this article: Liu L, Yang X, Yang J, Li G, Guo Y. Effect of hydrodynamic heterogeneity on micromixing intensification in a Taylor–Couette flow reactor with variable configurations of inner cylinder. *AIChE J*. 2021;e17225. https://doi.org/10.1002/aic.17225